ACS APPLIED MATERIALS & INTERFACES

Research Article

www.acsami.org

Electrochemical Determination of the Density of States of Nanostructured NiO Films

T. A. Nirmal Peiris,[†] Jagdeep S. Sagu,[†] K. G. Upul Wijayantha,[†] and Jorge García-Cañadas*[,‡]

[†]Department of Chemistry, Loughborough University, Loughborough LE11 3TU, United Kingdom

[‡]Cardiff School of Engineering, Cardiff University, The Parade, Cardiff CF24 3AA, United Kingdom

Supporting Information

ABSTRACT: Mesoporous p-type NiO films were prepared by aerosol-assisted chemical vapor deposition (AACVD) and characterized by X-ray diffraction (XRD). The nanostructure of the films was investigated by field emission gun scanning electron microscopy (FEG-SEM). The density of states (DOS) in these nanostructured films has been determined by means of electrochemical impedance spectroscopy and cyclic voltammetry. The analysis reveals an exponential distribution of band gap states above the valence band that extends around 1.5 eV. In addition, monoenergetic states were also identified which overlap with the exponential distribution. This distribution of states has an enormous influence in the electronic processes of the devices in which NiO electrodes are employed (electrochromism, water splitting or energy storage). Especially, in p-type dye-sensitized solar cells (p-DSCs), it is thought that intra-band-gap states are responsible for the fast observed recombination processes, whose existence and distribution has not been clearly determined yet and are now confirmed and quantified by our analysis. This provides a better comprehension of the recombination events which represent one of the main losses in p-DSCs.

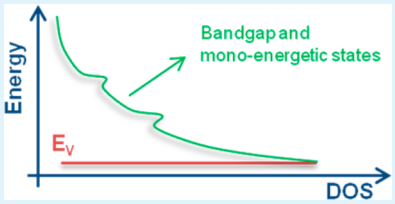

KEYWORDS: *cathodic dye-sensitized solar cells, chemical capacitance, geminate recombination, photocathode*

INTRODUCTION

Nanocrystalline nickel oxide (NiO) films have been considered for various applications, including energy storage,[1,2] electrochromism,[3,4] and photoelectrocatalysis,[5] due to its excellent electrochemical stability and ease of processing. In addition, it is the most investigated cathodic semiconductor to construct p-type dye-sensitized solar cells (p-DSCs).[5,6] NiO is typically deposited in the form of a film containing colloidal nanocrystals on top of a conducting substrate and then sintered to form a mesoporous rigid network with high internal surface area. In the case of p-DSCs, the nanocrystalline film is then sensitized with a light-absorbing dye and permeated with a redox electrolyte.

Nanostructured metal oxide films of semiconductors typically present a band gap distribution of states that plays an enormous role in the performance and dynamics of the devices.[7,8] The density of states (DOS) of a nanocrytalline semiconductor in the energy scale can be determined by a capacitive analysis of impedance spectroscopy (IS)[9] and cyclic voltammetry measurements[10] applied to a semiconductor/electrolyte junction that provides the chemical capacitance. Capacitive measurements frequently show two different contributions to the band gap DOS: an exponential tail that extends from the band edge toward the center of the band gap and monoenergetic states that overlap with the exponential distribution producing peaks.[11,12]

In NiO based p-DSCs, the main processes that limit the production of electricity are the very fast (geminate) recombination rate at the NiO/electrolyte interface and the low hole mobility.[5,13] The recombination is believed to occur via an intra-band-gap state which could lead to recombination in a stepwise fashion.[14] The hole transport is postulated to occur by a hopping mechanism between localized surface states, which also enhance the interfacial charge recombination losses.[15] To understand both processes and optimize the performance of the p-DSCs, it is clearly necessary to identify the DOS in the band gap, which is the main aim of this Article. To achieve this, we have prepared nanocryalline NiO films by aerosol-assisted chemical vapor deposition (AACVD), the phase purity of which was confirmed by X-ray diffraction (XRD) patterns. Field emission gun scanning electron microscope (FEG-SEM) images proved the nanocrystalline and mesoporous nature of the films. Cyclic voltammetry and impedance spectroscopy (IS) measurements have been employed to identify the chemical capacitance of the film and then extract the distribution of states.

EXPERIMENTAL SECTION

The NiO films were fabricated by the AACVD technique according to a previously reported method[16] onto fluorine-doped tin oxide (FTO) coated glass substrates (TEC 8 Pilkington, 8 Ω/□). Prior to the deposition, the FTO glass slides were ultrasonically cleaned sequentially using deionized water, propanol, deionized water, acetone, and ethanol for 15 min each. The AACVD precursor solution was prepared by heating and stirring nickel(II) acetylacetonate and 1 cm^3 of *N*,*N*-dimethylaminoethanol (to improve the solubility of the

Received: May 8, 2014
Accepted: August 19, 2014
Published: August 19, 2014

nickel(II) complex and to enhance volatility) in toluene for 30 min then allowing the solution to cool down to room temperature. In a typical deposition, a flask containing the precursor solution was placed above the piezoelectric modulator of an ultrasonic humidifier to generate an aerosol. Air at the rate of 210 mL min^{-1} was used as the carrier gas to transfer the aerosol to the deposition chamber through a second flask, where the large droplets were filtered from the aerosol stream, allowing only the fine aerosol droplets to be transferred to the deposition chamber, where it decomposed on the heated FTO substrate to form a nanocrystalline NiO film; the flow rate from the second flask was 2340 mL min^{-1}. The substrate temperature was maintained at 475 °C for 40 min during the deposition, after which they were removed from the hot plate surface and allowed to cool down to room temperature. All the chemicals were purchased from Sigma-Aldrich and used without further purification.

Phase and crystallinity of the deposited films were characterized using a Bruker D8 XRD operating with monochromatic intensity Cu Kα (λ = 1.54 Å) radiation using a position sensitive detector (PSD). Surface morphology of the NiO films was studied using a Leo 1530 VP FEG-SEM at an accelerating voltage of 5 kV and a working distance of 5 mm.

Electrochemical measurements were performed in a three-electrode electrochemical cell. The NiO film was used as the working electrode. Ag/AgCl in KCl 3 M and Pt electrodes served as reference and counter electrode, respectively. The electrolyte solution employed consisted of 0.1 M tetrabutylammonium perchlorate, 0.1 M tetrabutylammonium iodide and 0.5 M I_2 in acetonitrile. The immersed area, A, of the NiO electrode was 1 cm^2.

Cyclic voltammetry and IS measurements were performed using an Eco Chemie PGSTAT302N potentiostat. A 20 mV/s scan rate was used during the voltammetry experiments, and IS measurements were performed at 20 mV amplitude at different dc voltages in the 10 mHz to 15 kHz frequency range. Results were analyzed using Zview Software. The constant phase element was used in the fit to the equivalent circuits, and then chemical capacitance values were deduced using a previously reported procedure.[17]

RESULTS AND DISCUSSION

Chemical Characterization and Morphology of NiO Films. The powder XRD pattern of AACVD deposited NiO film on FTO glass is shown in Figure 1. The peaks indexed by

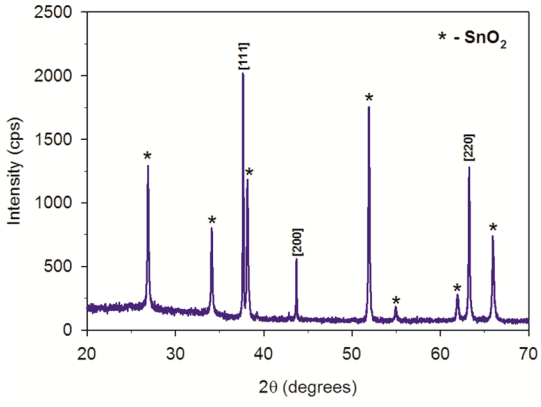

Figure 1. XRD pattern of NiO film deposited by AACVD at 475 °C for 40 min.

an asterisk (*) correspond to the SnO_2 layer of the glass substrate. The reflections of cubic NiO were analyzed and identified according to the International Centre for Diffraction Data (ICDD) powder diffraction file (PDF) number 47-1049. The sharp peaks at 37.5° and 63.2° correspond to the [111] and [220] reflections, and the less intense peak at 43.6° corresponds to the [200] reflection of the cubic NiO phase. This result confirmed the pure phase and the preferential orientation of NiO in the [111] direction in the films.

The morphology of the NiO films was investigated by using a FEG-SEM. The surface topographical and cross-sectional SEM images are shown in Figure 2a and b, respectively. The cross-sectional image shows that there are spikelike nanofeatures of NiO which are around 0.5 μm in height emerging from a compact layer of NiO. The compact layer is around 1 μm thick, and the overall film thickness is estimated to be about 1.5 μm. The surface topographical image (Figure 2a) shows that the nanofeatures are uniformly distributed and the diameter of each of them is ranging from 100 to 200 nm. In addition, it can be observed that the electrode is porous, with large pore sizes.

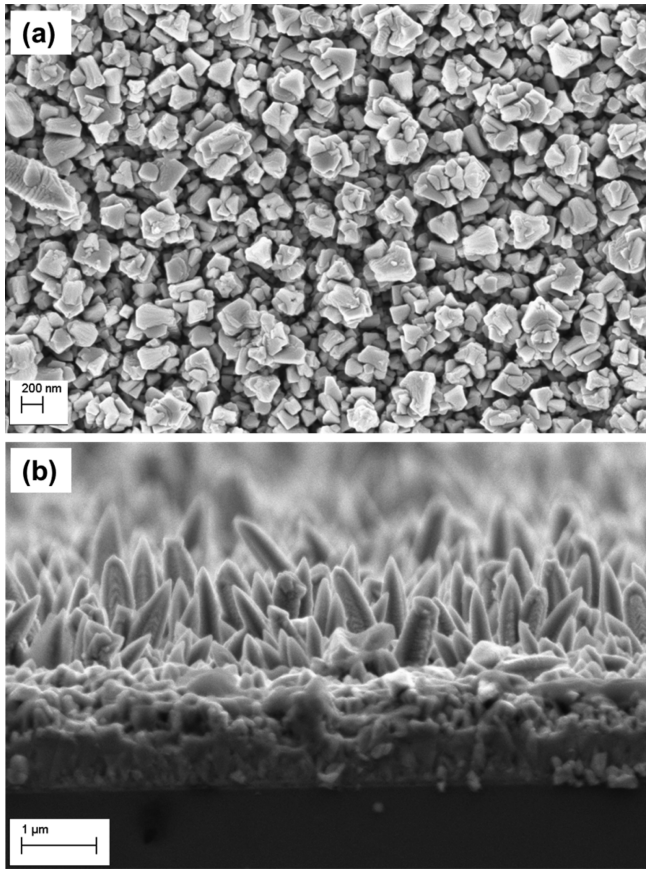

Figure 2. SEM images of NiO films deposited on FTO glass at 475 °C for 40 min. Surface topographical (a) and cross-sectional (b) images.

Electrochemical Analysis. The cyclic voltammograms of nanostructured metal oxide electrodes frequently show a symmetrical shape when no redox species are present in solution and thus all the carriers accumulate in the trap states available in the semiconductor band gap.[7,10] This accumulation of carriers in energetic states due to a variation of the Fermi level defines a chemical capacitance C_μ.[18] For example, in TiO_2 electrodes, an exponential increase of negative current occurs when the voltage is scanned toward negative values due to the filling of the trap states by electrons. When the scan is reversed toward more positive values, an exponential positive current rises due to the extraction of the previously accumulated carriers.[12] The symmetry of the voltammogram can frequently be distorted by the voltage drop due to the series resistance.[10] This trend has also been observed in mesoporous NiO.[19]

When electroactive molecules exist in the electrolyte, the accumulated carriers react oxidizing or reducing the redox species and the symmetrical feature of the voltammogram turns into a cathodic or anodic current which does not change sign when the scan direction is shifted. This feature was observed in the cyclic voltammogram of the NiO film (Figure 3). The

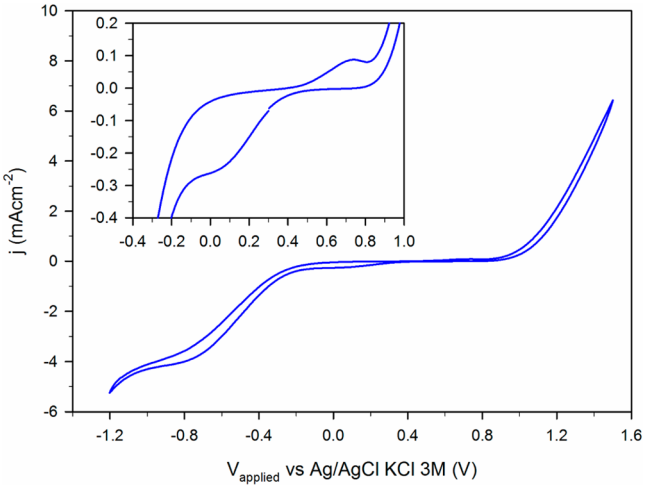

Figure 3. Cyclic voltammogram of NiO performed at 20 mV/s employing 0.1 M tetrabutylammonium perchlorate, 0.1 M tetrabutylammonium iodide, and 0.5 M I_2 electrolyte in acetonitrile. The inset shows a zoom to the mid-voltage region.

exponential cathodic and anodic currents are due to the reduction of I_2 and the oxidation of I_3^-, respectively. The inset of Figure 3 shows a close up of the mid-voltage region where two peaks can be observed, a minimum and a maximum around 0.1 and 0.7 V, respectively. This is usually due to the presence of monoenergetic states[11,12] which have been attributed to Ni(II), Ni(III), and Ni(IV) surface states.[19]

Analysis of the impedance results allows the quantification of the distribution of the band gap states. The impedance spectra obtained were fitted to an equivalent circuit consisting of a series resistance R_s connected in series with two semicircles in the more positive ($V_{app} \geq 1.2$ V) and negative ($V_{app} \leq -0.4$ V) applied voltage regions. The first semicircle corresponds to the parallel combination of the film capacitance (represented by a constant phase element) and the charge transfer resistance R_{ct} with the redox species. The second was attributed to the Warburg impedance Z_d which is observed when the faradaic reactions become controlled by the ionic diffusion of the redox species. At mid-voltages ($-0.4 < V_{app} < 1.2$ V), only the first semicircle was observed in series with R_s, except at $0.4 \leq V_{app} \leq 0.6$ V where a transmission element[20,21] due to the presence of transport resistance R_t in the film replaced the first semicircle. Some of the measured spectra at different dc voltages can be seen in Figure S1 in the Supporting Information.

Figure 4 shows the variation of the impedance parameters with the applied voltage. In Figure 4a, the feature of a chemical capacitance can be observed in the $-0.5 < V_{app} < 1.5$ V range. This is deduced from the large variation (around 2 orders of magnitude) experienced by the capacitance values, which renders unlikely the possibility of Mott-Shottky (dielectric) behavior at the FTO/electrolyte interface or a double layer (Helmhotlz) capacitance (usually 10−100 μF cm^{-2}) at the NiO/electrolyte junction.[21] The latter phenomenon begins to be observed at $V_{app} > 1.4$ V and is discussed below. In addition,

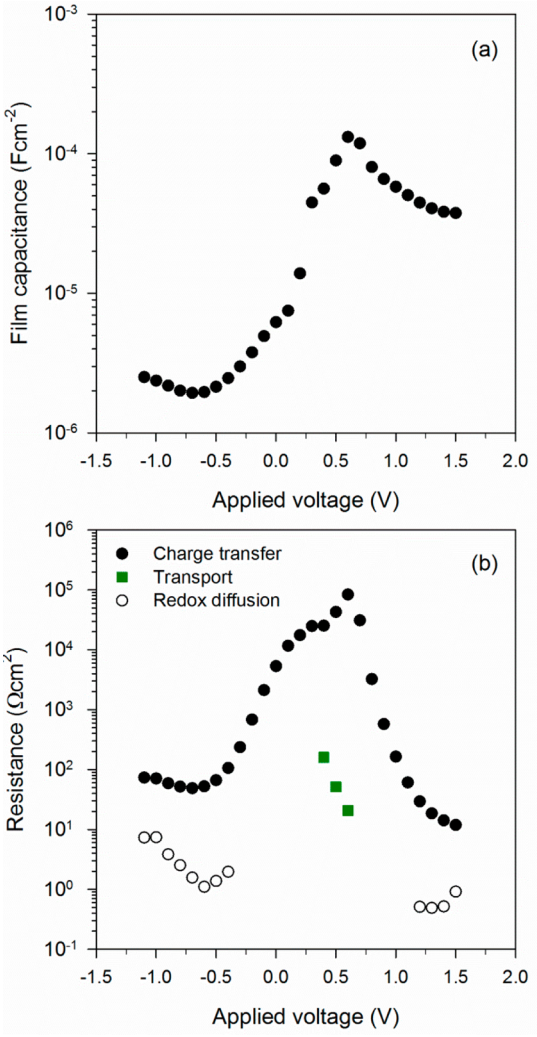

Figure 4. Film capacitance (a) and resistance values (b) obtained from impedance spectroscopy in the applied voltage range. In panel (b), the charge transfer (black circles), redox diffusion (white circles), and transport resistances (green squares) are distinguished.

the presence of the transport resistance (Figure 4b) at several voltages around 0.5 V, which decreases exponentially, indicates the variation of the carrier concentration in the valence band of NiO due to the shift of the Fermi level.

Three different regions can be identified in the voltage scale for the chemical capacitance. A clear exponential increase can be observed at $-0.5 \leq V_{app} \leq 0.1$ V, indicating the presence of an exponential distribution of band gap states which increases toward the valence band. An exponential increase was also identified for R_{ct} in this region (Figure 4b) due to the extraction of electrons from the NiO by the cathodic reaction $3I_2 + 2e^- \rightarrow 2I_3^-$. Second, a shoulder appears in Figure 4a at $0.1 < V_{app} < 0.5$ V due to the presence of monoenergetic states. This correlates with the minimum observed in R_{ct} (Figure 4b) and in the cyclic voltammogram (inset of Figure 3) at the same voltage region.

Finally, after the capacitive shoulder, a change of the current sign (from cathodic to anodic) was observed at $V_{app} \geq 0.6$ V in the dc current I_{dc} of the impedance and the cyclic voltammogram (Figure 3). This is due to the extinction of the cathodic reaction, governed by the concentration of electrons n in the film (chemical capacitance of electrons $C_{\mu n}$). On the other hand, the rise of the anodic oxidation ($2I_3^- + 2h^+ \rightarrow 3I_2$), is

dx.doi.org/10.1021/am502827z | ACS Appl. Mater. Interfaces 2014, 6, 14988−14993

controlled by the hole h^+ concentration p (chemical capacitance of holes $C_{\mu p}$). In contrast to the previous regions, an exponential decrease of $C_{\mu p}$ toward a constant value was observed when the potential was increased in this zone. This is due to the fact that p increases when the quasi-Fermi level of holes E_{Fp} decreases (applied voltage increase) unlike n which decreases when the electronic quasi-Fermi Level E_{Fn} is decreased. This is reflected in the opposite signs appearing in their definitions,[22]

$$C_{\mu p} = -e^2 \frac{dp}{dE_{Fp}} \quad (1)$$

$$C_{\mu n} = e^2 \frac{dn}{dE_{Fn}} \quad (2)$$

where e is the absolute charge of the electron. The trend of the capacitance toward a constant value is due to the large increase of the hole concentration in the film (E_{Fp} getting close to the valence band edge), which makes the reaction become controlled by the redox diffusion in the electrolyte (see the redox diffusion resistance values appearing in Figure 4b), and the accumulation of charge is governed by the Helmholtz capacitance at the NiO/electrolyte interface. The latter has a value of 37.6 μF cm^{-2} at 1.5 V, lying in the characteristic range (10−100 μF cm^{-2}) for this double layer capacitance[21] as mentioned previously. The R_{ct} decreases exponentially across several orders of magnitude (Figure 4b) in this more positive voltage region toward a constant value in agreement with the trend experienced by $C_{\mu p}$. The presence of additional monoenergetic states that could be expected from the small peak observed in the cyclic voltammogram around 0.7 V (Figure 3) was not clearly detected from Figure 4. However, it was observed later in the analysis.

In order to quantify the distribution of the DOS, the impedance parameters were plotted in Figure 5 against the internal or Fermi level voltage $V_F = -(E_{Fn} - E_{ref})/e$,[9] which is the actual voltage drop due to the variation of the quasi-Fermi level (E_{Fn}, or E_{Fp} when the current is anodic) with respect to the reference energy level E_{ref}. The internal voltage is calculated as $V_F = V_{app} - j_{dc}(R_s + R_t/3 + R_{diff})$, where $j_{dc} = I_{dc}/A$ is the dc current density and R_{diff} is the redox diffusion resistance in the electrolyte, extracted from the Warburg element. It can now be observed in Figure 5a the existence of a small minimum at $V_F \approx$ 0.8 V (also appearing around 0.7 V in the voltammogram of Figure 3) which relates to the presence of additional monoenergetic states in a position closer to the valence band edge.

The chemical capacitance per unit area can be defined using the approximation of the zero-temperature limit of the Fermi function as

$$C_\mu = (1 - a)Le^2 g(E_F) \quad (3)$$

where a is the film porosity, L is the thickness and $g(E_F)$ is the density of band gap states. Thus, C_μ provides a direct reading of the DOS when E_F is scanned in the energy scale. For an exponential distribution, the DOS that extends toward the valence band edge E_v is given by[18]

$$g(E_F) = \frac{\alpha N_L}{kT} \exp[\alpha(E_v - E_F)/kT] \quad (4)$$

where α is a parameter related with the band gap distribution, N_L is the total number of trap states above the valence band for the whole film volume, k is the Boltzmann constant, and T is the absolute temperature. Using the definition of the internal voltage ($V_F = -(E_{Fn} - E_{ref})/e$) and eq 4, eq 3 takes the form

$$C_\mu = C_o \exp\left(\frac{\alpha e}{kT} V_F\right) \quad (5)$$

with

$$C_o = (1 - a)Le^2 \frac{\alpha N_L}{kT} \exp[\alpha(E_v - E_{ref})/kT] \quad (6)$$

In the more negative voltage region of the capacitance (Figure 5a, black circles), the exponential feature predicted by eq 5 is observed with a value $\alpha = 0.067$ at $T = 300$ K extracted from the exponential fit. A similar behavior occurs in the more positive voltage part (Figure 5a, white circles) with $\alpha = 0.059$ at the same T, which is slightly lower than in the first region due to the influence of the monoenergetic states. It should be noted that the parameter accounting for the spread of the distribution is less pronounced than in other mesoporous electrodes such as TiO_2 where values of $\alpha \approx 0.3$ are typically observed,[23]

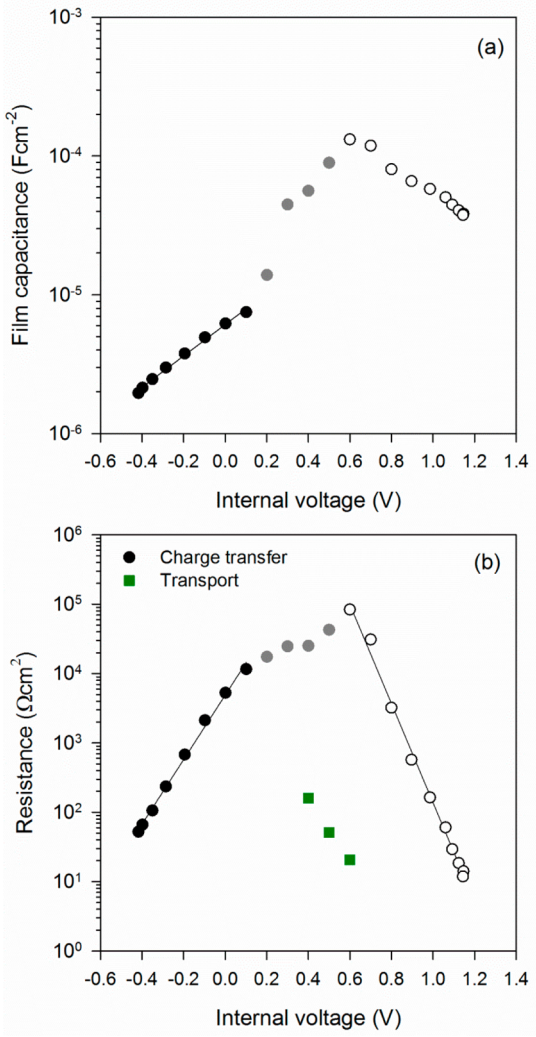

Figure 5. Film capacitance (a) and resistance values (b) vs the internal or Fermi level voltage ($V_F = V_{app} - j_{dc}(R_s + R_t/3 + R_{diff})$. In panel (b), the charge transfer (circles) and transport (squares) resistances can be distinguished. The three different voltage regimes analyzed are represented by black, gray, and white circles. Solid lines represent exponential fits.

producing variations of around 2 orders of magnitude in the chemical capacitance within 0.3 eV change of the quasi-Fermi level. In the case of NiO, a change of 2 orders of magnitude requires 1 eV variation. There is also a remarkably large extension in the energy scale of the band gap distribution, to around 1.5 eV. This has an important relevance in the dynamics of p-DSCs as discussed below.

In the central region (Figure 5a, gray circles), the existing monoenergetic states cause a more significant influence in the chemical capacitance and R_{ct} than in the more positive voltage region and thus clear peaks are observed in Figure 5. This stronger influence can also be appreciated in the cyclic voltammogram in Figure 3.

The charge transfer resistance of the band gap states with the electrolyte is given by[9]

$$R_{ct} = R_0 \exp\left(-\frac{\beta e}{kT} V_F\right) \tag{7}$$

with

$$R_o = \frac{\sqrt{\pi\lambda kT}}{e^2 L \alpha k_r c_{redox} N_s} \exp\left[\alpha \frac{(E_v - E_{redox})}{kT} + \frac{\lambda}{4kT}\right] \tag{8}$$

with c_{redox} being the concentration of acceptor (I_2 for the cathodic reaction) or donor species (I_3^- for the anodic reaction) in the electrolyte, λ being the reorganization energy of the acceptor species, N_s being the total number of band gap states contributing to the charge transfer, k_r being the rate constant accounting for the kinetics of the reaction, E_{redox} being the energetic redox level in the electrolyte, and β being a coefficient accounting for nonlinear charge transfer.[24] The clear exponential trends shown in Figure 5b for the more negative and more positive voltage regions were fitted using eq 7, which provided $\beta = 0.27$ and $\beta = 0.55$ respectively. These values show a nonlinear charge transfer behavior ($\beta < 1$) and a very distinctive reaction kinetics for the two different species involved (I_3^- and I_2).

Implications of the DOS in the Performance of p-DSCs. In p-type DSCs based on NiO, two main recombination paths have been proposed.[5] First, the injected holes in the valence band can react with I^- species in the electrolyte. This anodic reaction relates to the more positive voltage region of our analysis (white circles in Figure 5), and as it was observed it can take place via both the band gap and the extended states of the valence band. It would be expected to predominantly occur via the trap distribution for cells with low photovoltages which is the region where the hole chemical capacitance is governed by the band gap distribution. However, the influence of the valence band is expected to appear quickly since the transport resistance becomes negligible at voltages very close to the rise of the anodic reaction (Figure 4b), indicating a sufficient hole concentration to provide proper hole conductivity.

The second recombination path is related to the capture of the excited electron in the sensitizer by the NiO instead of the redox mediator. In principle, this would be presumably hindered since the lowest unoccupied molecular orbital (LUMO) is energetically very far from the valence band edge.[13] However, the wide extent of the trap distribution observed in Figure 3a implies the existence of band gap states even at negative voltages. These states can overlap with the LUMO level, which could facilitate the electron injection into the NiO traps. Once injected, the electron may recombine with the injected hole in the valence band within the NiO in a stepwise fashion[5] or with the I_3^- redox species. On the other hand, the injection of the excited electron in addition to the photogenerated hole would significantly decrease the photovoltage.

CONCLUSIONS

The distribution of the DOS of a mesoporous NiO film prepared by AACVD has been analyzed by electrochemical methods. Chemical and structural characterizations of NiO films were carried out via XRD and FEG-SEM, respectively. The data confirmed the pure phase and porous structure of the deposited NiO film. The presence of an exponential tail of band gap states has been identified by analyzing the film capacitance obtained by impedance spectroscopy. The distribution grows toward the valence band edge and extends ~1.5 eV. In addition, two monoenergetic state distributions were observed which are responsible for the peaks observed in the cyclic voltammogram and in the charge transfer resistance and chemical capacitance.

The quantification of the DOS sets the basis for the proper understanding of key processes in devices in which mesoporous NiO films are utilized. In the case of p-type DSCs, many researchers believe that the recombination and hole transport takes place via band gap states. The presence of a trap tail has been confirmed by our study, and due to the large extent of the distribution of states coupling between traps and the LUMO of the sensitizer, both quite far in the energy scale from the valence band edge, becomes possible. This is probably the origin of the very fast (geminate) recombination.

ASSOCIATED CONTENT

Supporting Information

Representative impedance measurements at different dc voltages. This material is available free of charge via the Internet at http://pubs.acs.org/.

AUTHOR INFORMATION

Corresponding Author

*E-mail: jorge.garcia.canadas@gmail.com.

Notes

The authors declare no competing financial interest.

ACKNOWLEDGMENTS

The authors T.A.N.P. and K.G.U.W. acknowledge the support received from Johnson Matthey Plc. and RCUK.

REFERENCES

(1) Wang, Y. G.; Xia, Y. Y. Electrochemical Capacitance Characterization of NiO with Ordered Mesoporous Structure Synthesized by Template Sba-15. *Electrochim. Acta* **2006**, *51*, 3223−3227.

(2) Liu, H.; Wang, G. X.; Liu, J.; Qiao, S. Z.; Ahn, H. J. Highly Ordered Mesoporous NiO Anode Material for Lithium Ion Batteries with an Excellent Electrochemical Performance. *J. Mater. Chem.* **2011**, *21*, 3046−3052.

(3) Xia, X. H.; Tu, J. P.; Zhang, J.; Wang, X. L.; Zhang, W. K.; Huang, H. Electrochromic Properties of Porous NiO Thin Films Prepared by a Chemical Bath Deposition. *Sol. Energy Mater. Sol. Cells* **2008**, *92*, 628−633.

(4) Niklasson, G. A.; Granqvist, C. G. Electrochromics for Smart Windows: Thin Films of Tungsten Oxide and Nickel Oxide, and Devices Based on These. *J. Mater. Chem.* **2007**, *17*, 127−156.

(5) Odobel, F.; Pellegrin, Y. Recent Advances in the Sensitization of Wide-Band-Gap Nanostructured P-Type Semiconductors. Photovoltaic and Photocatalytic Applications. *J. Phys. Chem. Lett.* **2013**, *4*, 2551−2564.

(6) Nattestad, A.; Mozer, A. J.; Fischer, M. K. R.; Cheng, Y. B.; Mishra, A.; Bauerle, P.; Bach, U. Highly Efficient Photocathodes for Dye-Sensitized Tandem Solar Cells. *Nat. Mater.* **2010**, *9*, 31−35.
(7) Bisquert, J.; Fabregat-Santiago, F.; Mora-Sero, I.; Garcia-Belmonte, G.; Barea, E. M.; Palomares, E. A Review of Recent Results on Electrochemical Determination of the Density of Electronic States of Nanostructured Metal-Oxide Semiconductors and Organic Hole Conductors. *Inorg. Chim. Acta* **2008**, *361*, 684−698.
(8) Anta, J. A.; Mora-Sero, I.; Dittrich, T.; Bisquert, J. Dynamics of Charge Separation and Trap-Limited Electron Transport in TiO_2 Nanostructures. *J. Phys. Chem. C* **2007**, *111*, 13997−14000.
(9) Fabregat-Santiago, F.; Garcia-Belmonte, G.; Mora-Sero, I.; Bisquert, J. Characterization of Nanostructured Hybrid and Organic Solar Cells by Impedance Spectroscopy. *Phys. Chem. Chem. Phys.* **2011**, *13*, 9083−9118.
(10) Fabregat-Santiago, F.; Mora-Sero, I.; Garcia-Belmonte, G.; Bisquert, J. Cyclic Voltammetry Studies of Nanoporous Semiconductors. Capacitive and Reactive Properties of Nanocrystalline TiO_2 Electrodes in Aqueous Electrolyte. *J. Phys. Chem. B* **2003**, *107*, 758−768.
(11) Bertoluzzi, L.; Herraiz-Cardona, I.; Gottesman, R.; Zaban, A.; Bisquert, J. Relaxation of Electron Carriers in the Density of States of Nanocrystalline TiO_2. *J. Phys. Chem. Lett.* **2014**, *5*, 689−694.
(12) Berger, T.; Monllor-Satoca, D.; Jankulovska, M.; Lana-Villarreal, T.; Gómez, R. The Electrochemistry of Nanostructured Titanium Dioxide Electrodes. *ChemPhysChem* **2012**, *13*, 2824−2875.
(13) Morandeira, A.; Boschloo, G.; Hagfeldt, A.; Hammarström, L. Coumarin 343−NiO Films as Nanostructured Photocathodes in Dye-Sensitized Solar Cells: Ultrafast Electron Transfer, Effect of the I_3^-/I^- Redox Couple and Mechanism of Photocurrent Generation. *J. Phys. Chem. C* **2008**, *112*, 9530−9537.
(14) Smeigh, A. L.; Pleux, L. L.; Fortage, J.; Pellegrin, Y.; Blart, E.; Odobel, F.; Hammarstrom, L. Ultrafast Recombination for NiO Sensitized with a Series of Perylene Imide Sensitizers Exhibiting Marcus Normal Behaviour. *Chem. Commun.* **2012**, *48*, 678−680.
(15) Natu, G.; Hasin, P.; Huang, Z. J.; Ji, Z. Q.; He, M. F.; Wu, Y. Y. Valence Band-Edge Engineering of Nickel Oxide Nanoparticles via Cobalt Doping for Application in p-Type Dye-Sensitized Solar Cells. *ACS Appl. Mater. Interfaces* **2012**, *4*, 5922−5929.
(16) Sialvi, M. Z.; Mortimer, R. J.; Wilcox, G. D.; Teridi, A. M.; Varley, T. S.; Wijayantha, K. G. U.; Kirk, C. A. Electrochromic and Colorimetric Properties of Nickel(II) Oxide Thin Films Prepared by Aerosol-Assisted Chemical Vapor Deposition. *ACS Appl. Mater. Interfaces* **2013**, *5*, 5675−5682.
(17) Proskuryakov, Y. Y.; Durose, K.; Al Turkestani, M. K.; Mora-Sero, I.; Garcia-Belmonte, G.; Fabregat-Santiago, F.; Bisquert, J.; Barrioz, V.; Lamb, D.; Irvine, S. J. C.; Jones, E. W. Impedance Spectroscopy of Thin-Film CdTe/Cds Solar Cells under Varied Illumination. *J. Appl. Phys.* **2009**, *106*, 44507−44507−9.
(18) Bisquert, J. Chemical Capacitance of Nanostructured Semiconductors: Its Origin and Significance for Nanocomposite Solar Cells. *Phys. Chem. Chem. Phys.* **2003**, *5*, 5360−5364.
(19) Marrani, A. G.; Novelli, V.; Sheehan, S.; Dowling, D. P.; Dini, D. Probing the Redox States at the Surface of Electroactive Nanoporous NiO Thin Films. *ACS Appl. Mater. Interfaces* **2013**, *6*, 143−152.
(20) Fabregat-Santiago, F.; Bisquert, J.; Palomares, E.; Otero, L.; Kuang, D. B.; Zakeeruddin, S. M.; Gratzel, M. Correlation Between Photovoltaic Performance and Impedance Spectroscopy of Dye-Sensitized Solar Cells Based on Ionic Liquids. *J. Phys. Chem. C* **2007**, *111*, 6550−6560.
(21) Herraiz-Cardona, I.; Fabregat-Santiago, F.; Renaud, A.; Julián-López, B.; Odobel, F.; Cario, L.; Jobic, S.; Giménez, S. Hole Conductivity and Acceptor Density of P-Type $CuGaO_2$ Nanoparticles Determined by Impedance Spectroscopy: The Effect of Mg Doping. *Electrochim. Acta* **2013**, *113*, 570−574.
(22) Mora-Seró, I.; Luo, Y.; Garcia-Belmonte, G.; Bisquert, J.; Muñoz, D.; Voz, C.; Puigdollers, J.; Alcubilla, R. Recombination Rates in Heterojunction Silicon Solar Cells Analyzed by Impedance Spectroscopy at Forward Bias and under Illumination. *Sol. Energy Mater. Sol. Cells* **2008**, *92*, 505−509.
(23) Raga, S. R.; Barea, E. M.; Fabregat-Santiago, F. Analysis of the Origin of Open Circuit Voltage in Dye Solar Cells. *J. Phys. Chem. Lett.* **2012**, *3*, 1629−1634.
(24) Bisquert, J.; Mora-Seró, I. Simulation of Steady-State Characteristics of Dye-Sensitized Solar Cells and the Interpretation of the Diffusion Length. *J. Phys. Chem. Lett.* **2009**, *1*, 450−456.